Journal of Inflammation Research

Dovepress
Taylor & Francis Group

Open Access Full Text Article

ORIGINAL RESEARCH

Medical Hemorrhoid Gel Ameliorates Croton Oil-Induced Hemorrhoids by Suppressing the NLRP3 Inflammasome Activation via NF-κB Signaling Pathway

Zhongzhu Ai[1,2,*], Dongfeng Yuan[3,*], Yun Li[3], Jingyi Cai[3], Daonian Zhou[2], Wei Liu[2]

[1]Department of Pharmaceutics, School of Pharmaceutical Science, Peking University, Beijing, 100191, People's Republic of China; [2]Post-Doctoral Research Center, Mayinglong Pharmaceutical Group Co., Ltd, Wuhan, 430070, People's Republic of China; [3]School of Pharmacy, Hubei University of Chinese Medicine, Wuhan, 430065, People's Republic of China

*These authors contributed equally to this work

Correspondence: Wei Liu; Daonian Zhou, Email lw165271351@163.com; zdn81@163.com

Background: Hemorrhoidal disease (HD) is characterized by the pathological dilation of anal vascular cushions, causing pain, itching and bleeding. Recent evidence links HD onset and progression to rectal inflammation. Medical Hemorrhoid Gel (MHG), a multi-component botanical preparation, has gained empirical validation for HD management. This study aims to systematically evaluate the safety, efficacy, and mechanism of action of MHG in treating HD.

Methods: The phytochemical composition of MHG was characterized using UPLC-QTOF-MS/MS and GC-MS/MS analyses. In vivo, the efficacy was assessed in a croton oil preparation (COP)-induced HD rat model (n=10 per group) via anorectal coefficient (ARC) measurement, macroscopic severity score, Evans blue extravasation quantification, and H&E/PAS staining. Transcriptomic sequencing of anorectal tissues was integrated with experimental validation using ELISA, immunohistochemistry (IHC), and Western blotting to delineate molecular mechanism. Data were analyzed by one-way analysis of variance (ANOVA) followed by Dunnett's multiple comparison post hoc test (significance at $p<0.05$).

Results: MHG significantly reduced ARC, macroscopic severity score, and Evans blue extravasation, restored intestinal villus structure and goblet cell numbers, and alleviated inflammation. Acute toxicity tests showed that MHG did not cause anorectal abnormalities or systemic toxicity in rats. Transcriptomic analysis integrated with experimental validation suggested the therapeutic mechanism of MHG involves inflammation response and NF-κB pathway. Specifically, MHG suppressed the levels of the pro-inflammatory mediator TNF-α, while it enhanced the levels of the anti-inflammatory mediator IL-10. Mechanistic studies revealed that MHG inhibited NLRP3 inflammasome activation, reduced the phosphorylation level of p65 and enhanced IκBα expression. Phytochemical analysis identified 20 constituents that contribute to the bioactivity of MHG.

Conclusion: Our study substantiated that MHG exerts anti-hemorrhoidal effects through NLRP3 inflammasome suppression via NF-κB pathway regulation. This mechanistic insight provides scientific validation for clinical application of MHG in HD management.

Keywords: medical hemorrhoid gel, hemorrhoidal disease, inflammation, NLRP3 inflammasomes, NK-κB signaling pathway

Introduction

HD is a common anorectal disorder characterized by the pathological dilation of the hemorrhoidal vascular cushions. The global prevalence of HD is alarmingly high, with some reports up to 86%.[1] HD imposes a considerable healthcare and socioeconomic burden, with an estimated annual cost of $800 million in the United States alone.[2] Characteristic clinical manifestations including painful swelling, persistent pruritus, and recurrent bleeding, impair patients' quality of life.[3] Emerging evidence implicated that dysregulated inflammatory mediators (eg TNF-α, IL-6, and COX-2), are key factors in the pathogenesis of HD.[4] Moreover, increasing studies have found that activation of the NLRP3/NF-κB axis in the

Received: 6 March 2025
Accepted: 5 July 2025
Published: 7 August 2025

intestinal further promotes the inflammatory response by upregulating pro-inflammatory cytokines, thereby exacerbating HD progression.[5] Current therapies include surgical interventions for advanced cases and pharmacological therapies for mild to moderate cases.[6,7] Among these therapies, certain standardized plant extracts, such as European chestnut seed extract (*Castanea sativa* Mill., marketed as Aescuven forte®) and micronized purified flavonoid fraction (marketed as Daflon®) have shown significant clinical efficacy.[8,9] In addition, a randomized Phase II clinical trial demonstrated that, compared with a topical chemical agent, flavonoid lotion significantly improved hemorrhoidal symptoms, with favorable safety and accessibility.[10] These studies underscore the great potential of herbal therapies in hemorrhoid management.

MHG, a botanical preparation (Registration No: Xiang Xie Zhu Zhun 20192140219), is formulated by blending *Hamamelis mollis* Oliv. extract, borneolum syntheticum (*Cinnamomum camphora (L)*. Presl), and recombinant collagen in a 50:40:5 ratio. Clinically, MHG has been used to treat HD successfully in China, and achieved a market sales exceeding RMB 100 million in 2024. Traditionally, both *Hamamelis mollis* Oliv and borneolum syntheticum are integral components of many folk anti-hemorrhoidal preparation,[11,12] suggesting that they are likely the primary active components contributing to its effects. *Hamamelis mollis* Oliv origins from the root of *Hamamelis mollis* Oliv and is documented in classic medical works such as *Xin Hua Ben Cao Gang Yao* and *Zhong Hua Ben Cao*. It is used to manage conditions such as eczema, varicose veins, and hemorrhoids. Pharmacological evidence showed that it can promote blood circulation and exhibits antimicrobial properties, which contribute to the early intervention of HD.[13] Borneolum syntheticum is derived from the fresh branches and leaves of *Cinnamomum camphora (L)*. Presl and is documented in ancient works such as *Tang Bencao, and Bencao Gangmu*. It is renowned for its abilities to reduce swelling and relieve pain, effectively treating conditions such as tongue swelling, hemorrhoids, and oral ulcers. Additionally, borneolum syntheticum possesses strong anti-inflammatory effects, and it can also enhance skin permeability, improving the absorption of active ingredients in the formulation.[14,15] Recombinant collagen has significant regenerative effects by reducing inflammation, accelerating collagen deposition, and promoting vascular regeneration, and its excellent biocompatibility enhances drug bioavailability and therapeutic efficacy.[16,17] Moreover, our previous research further confirmed the effect of MHG in improving hemorrhoidal swelling and itching by in vivo studies.[18] However, the main pharmacological actions of MHG against HD remain less well described. Elucidating how MHG regulates key pathways could help identify new therapeutic targets for HD, guide the optimization of botanical formulations, and facilitate the development of synthetic analogs. Herein, we established a rat hemorrhoidal model induced by COP to analyze the underlying mechanisms of MHG through integrating pharmacodynamic and bioinformatics approach. These findings will provide the preliminary experimental evidence supporting the clinical application of MHG. The research process of this study is illustrated in Figure 1.

Materials and Methods

Drugs and Chemicals

Titanoreine Cream (TC, Lot No. NEJS235) was purchased from Xi'an Yangsen Pharmaceutical Co., Ltd (Xi'an, China) and was selected as the positive drug for this study. Croton oil (Lot No.C13225402) was provided from Shanghai Macklin Biochemical Technology Co., Ltd (Shanghai China). Formamide (Lot No. C14418678) and pyridine (Lot No. P11511) were obtained from Shanghai Aladdin Biochemical Technology Co., Ltd (Shanghai, China). Evans blue (Lot No. 23089145) was provided by Biosharp (Beijing China).

Preparation of MHG

MHG was provided by Hunan Renxin Biotechnology Co., Ltd (Changsha China). Its basic components include *Hamamelis mollis* Oliv extract, borneolum syntheticum, recombinant collagen, and other excipients. The preparation process is briefly described as follows: First, *Hamamelis mollis* Oliv was extracted with 50% concentration of ethanol, filtered and concentrated. Hamamelitannin, kaempferol and gallic acid served as quality markers, and the extract was tested by HPLC to ensure compliance with established quality standards, yielding *Hamamelis mollis* Oliv extract. Second, borneolum syntheticum is ground into a low-melting-point liquid and fully dissolved in glycerin to obtain the borneol solution. Third, the *Hamamelis mollis* Oliv extract, borneol solution, and recombinant collagen are mixed with

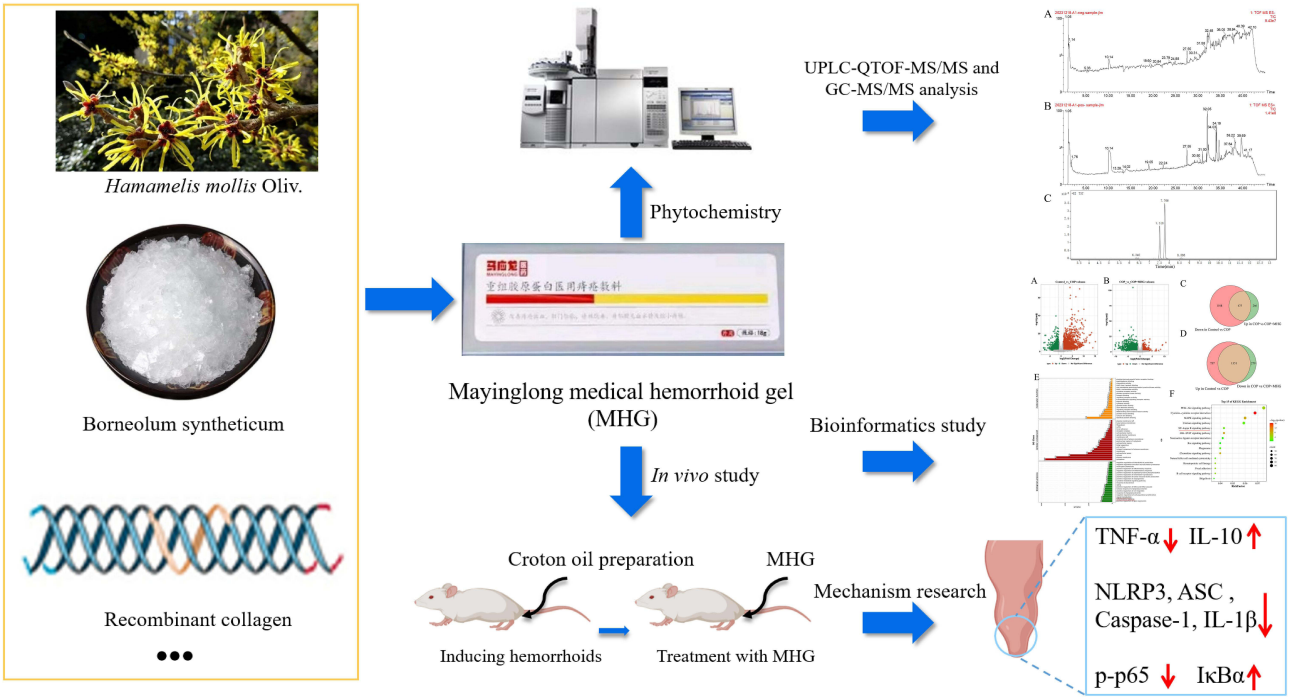

Figure 1 Flow chart of research scheme of MHG.

other excipient at a ratio of 50:40:5 to formulate MHG. The production of MHG strictly adheres the Chinese GMP certification standard and is manufactured by Hunan Renxin Biotechnology Co., Ltd. All products undergo batch-specific sampling inspections and must meet predefined quality control criteria before market release. The batch number of MHG used in this experiment is Lot No. 20230103.

Animals Study

One hundred and ten male SD rats (SPF-grade) aged 6–8 weeks and weighing 200–220 g were sourced from the Henan Skobes Biotechnology Co., Ltd. (NO. SYXK (Hubei) 2017–0067), and housed four-five rats in independently vented at the animal facility of the Hubei University of Chinese Medicine. The animals were treated in accordance with the Guidelines for Ethical Review of Experimental Animal Welfare (GB/T35892-2018) issued by China. The experimental protocol was approved by the Animal Ethics Committee of Hubei University of Chinese Medicine.

HD model was induced according to the procedure described previously.[19] Briefly, COP was prepared by mixing deionized water, pyridine, ether, and a 6% solution of croton oil in ether at a ratio of 1:4:5:10. Prior to COP administration, the rats were fasted overnight. A 0.16 mL of COP was then injected approximately 2–3 cm deep into the anus of rats and held for 8–10 seconds to prevent leakage. Anal swelling was monitored following COP application.

In the present study, animal experiments were conducted in two phases. First, sixty rats were used for safety, efficacy and mechanism investigations (Permission No. SYXK2017-0067-ZYZYZX2023-031). The ten rats were used for the safety text of MHG, and the detailed experimental procedures can be seen in the supplementary information 1. The fifty rats were randomly assigned to five groups (n = 10): (1) Control, (2) COP, (3) COP + MHG (0.5 g/kg), (4) COP + MHG (1.0 g/kg), and (5) COP + TC (1.0 g/kg). The equivalent doses for rats were calculated by adjusting the human dose based on body weight. Specifically, the commonly used clinical dosage range of MHG is 3.0–6.0 g/day. After dosage conversion, we obtained the equivalent dose for rats to be 0.315–0.63 g/kg. Given the results of preliminary experiments, the high and low doses of MHG were set as 1.0 g/kg and 0.5 g/kg, respectively, while the dose of TC was set as 1.0 g/kg. HD was induced in all groups except the Control group via rectal injection of COP. After 30 minutes, significant swelling was observed in the anuses of rats. Then, the respective drugs were administered through a rectal catheter inserted 2 cm into the anus and maintained for 30 s to prevent drug leakage. Swelling peaked after 8 h of exposure to COP.

Subsequently, the rats were euthanized under anesthesia, and anorectal tissue samples were collected for further analysis. Second, the remaining fifty rats were grouped and treated in the same way to study Evans blue extravasation (Permission No. SYXK2017-0067-ZYZYZX2023-051).

Hemorrhoids Evaluation

Measurement of Anorectal Coefficient (ARC)

After euthanasia, the rats were dissected, and tissue samples from the anorectal region, each measuring 20 mm in length, were collected and weighed. The ARC was then calculated using the following formula:

$$ARC = \frac{\text{Weight of anorectal tissue(mg)}}{\text{Body weight of Rat(g)}}$$

Assessment of Macroscopic Severity Score

The tissue samples were fixed on ordinary paper, and the macroscopic severity of the anorectal tissue was assessed and recorded as previously described.[20] Briefly, the observations and scoring were conducted by two experienced independent reviewers (Z. Ai and D. Yuan) who were fully blinded to the treatment groups. The assessment criteria included degree of anal swelling, the extent of rectal mucosal damage, color intensity, and tissue elasticity. The scoring system ranges from 0 to 2, detailed as follows: normal (0), tissue appears normal in color with no abnormal vascular dilation or surface damage; mild symptoms (1), tissue exhibits slight inflammation or swelling with a reddish discoloration; severe symptoms (2), tissue shows significant inflammation, swelling, or even bleeding.

Evaluation of Evans Blue Extravasation

The Evans blue exudation was employed to assess vascular permeability of rectal tissue according to the method described previously.[19] Briefly, rats were anesthetized and injected with Evans blue dye through the tail vein at a dose of 40 mg/kg. After 1 hour, the rats were euthanized, and 2 cm sections of anorectal tissue were dissected and weighed. The tissue samples in centrifuge tubes containing 1 mL of formamide and incubated at 55°C for 24 hours to extract the Evans blue dye. Absorbance was measured at 620 nm using a Tecan Spark10M multi-mode microplate reader (Tecan, Switzerland), with formamide serving as the blank control. The Evans blue content in each sample was calculated using a standard curve generated from various concentrations of Evans blue solution. The calculation formula is as follows: Evans blue exudation rate=Evans Blue Content (μg)/Weight of anorectal tissue (g).

Histopathology Analysis of Anorectal Tissue

After fixation in 4% paraformaldehyde for 24 hours, fresh tissue samples from the anorectal region were sliced into 4 mm thick sections using an automatic rotary microtome (Lot No. RM2016, Leica, Germany). These sections were then embedded in paraffin wax for further analysis, including staining with Hematoxylin and Eosin (HE) (Lot No. S191003, Pinofi Biotechnology Co., Ltd, China) and Periodic Acid-Schiff (PAS) (Lot No. S191008, Pinofi Biotechnology Co., Ltd, China).

RNA-Seq

Following the manufacturer's guidelines, total RNA was extracted from anorectal tissues using the Total RNA Kit I (Lot No. R6834, Omega, USA). The concentration of the extracted total RNA was determined using a NanoDrop One spectrophotometer (NanoDrop Technologies, Germany), and RNA quality was assessed by electrophoresis. Subsequently, cDNA libraries were prepared and quantified using a Qubit 2.0 Fluorometer (Life Technologies, USA), followed by evaluation on an Agilent 2100 bioanalyzer (Agilent Technologies, USA). Samples meeting the required quality standards were processed for sequencing on the Illumina Novaseq 6000 platform (Illumina, USA).

Subsequently, the raw fastq data were filtered using fastp (version: 0.21.0) (https://github.com/OpenGene/fastp) to obtain valid data. Quality control of the filtered data was conducted using fastqc (version: 0.11.9). After filtration, Star 2.7.9a alignment software (https://github.com/alexdobin/STAR) was used for alignment of transcriptome sequences with

reference genome (version: mRatBN7.2). The alignment results were visualized and browsed using the Integrative Genomics Viewer (IGV).

DESeq2 (version: 1.26.0) was used to analyze and identify differentially expressed genes (DEGs), applying screening criteria of $|\log_2 FC| > 1$ and p-value < 0.05. Using clusterProfiler (version: 3.14.3), we performed Gene Ontology (GO) and KEGG Pathway enrichment analyses on the DEGs. Data visualization was performed using the bioinformatics platform (https://www.bioinformatics.com.cn/).

ELISA Detection

Following the manufacturer's guidelines, ELISA kits specific for rat TNF-α (Lot No. DP0326808173, Elabscience, China) and rat IL-10 (Lot No. UX138PL45277, Elabscience, China) were employed to measure the concentrations of these substances in rat anorectal tissue.

IHC Analysis

After dewaxing the tissue sections, antigen retrieval was performed using 1× citrate buffer (pH 6.0) (Lot No. 10007108, Sinopharm Chemical Reagent Co., Ltd, China) under high temperature and pressure for 2 minutes. The samples were then cooled to room temperature. To block endogenous peroxidase activity, sections were treated with a 3% H2O2 solution at room temperature for 20 minutes, followed by three washes with PBS. Subsequently, goat serum (10%) was applied to the tissues and incubated at 37°C for 30 minutes. Next, the tissue sections were incubated overnight at 4°C with specific antibodies against NLRP3, p-p65, p65, ASC (Abways, China), Caspase-1 (Bioss, China), and IκBα (Abclonal, China). Following primary antibody incubation, HRP-conjugated secondary antibodies (Pinofi Biotechnology Co., Ltd, China) were applied and incubated at 37°C for 1 hour. The sections were washed three times with PBST, stained with DAB substrate, rinsed with water to remove excess DAB staining solution, and counterstained with hematoxylin solution (Lot No. P0064, Pinofi Biotechnology Co., Ltd, China). Finally, sections were sealed with an appropriate amount of neutral gum (Lot No. 10004160, Sinopharm Chemical Reagent Co., Ltd, China).

Western Blotting Assay

After homogenizing adequate anorectal tissue to extract total protein, the concentration of protein was determined using the BCA Protein Quantification Kit (Gbcbio Technologies, China). The protein was separated using SDS-PAGE electrophoresis. Target protein bands were identified using markers and transferred onto PVDF membranes. The PVDF membranes were then blocked for two hours, followed by overnight incubation at 4°C with primary antibodies: anti-TNF-α, anti-NLRP3, anti-caspase-1, anti-p65, anti-p-p65, anti-IκBα (Affinity, USA), anti-IL-1β (GeneTex, USA), anti-ASC (Bioss, China), anti-Pro-caspase-1 (Abcam, UK), anti-IL-10, and anti-β-actin (Proteintech, China). Subsequently, the membranes were incubated with HRP-conjugated secondary antibodies (diluted 1:10,000) for two hours. After washing off excess secondary antibodies, the solution mixture composed of ECL reagent (Lot No. KF8003, Affinity, USA) and peroxidase solution (1:1 ratio) was applied to the PVDF membrane. The reaction was allowed to proceed for several minutes until the fluorescence bands became apparent, excess solution was removed using filter paper. The membrane was then covered with plastic wrap, and the X-ray (Kodak, USA) film was placed on top. The film was subsequently developed and fixed using developer and fixer reagent kit (Tianjin Hanzhong Photography Materials Factory, China). Finally, the developed film was rinsed, air-dried, and scanned. The Image J software was employed to analyze grayscale value, with β-actin serving as the internal reference.

Phytochemical Analysis of MHG

UPLC-QTOF-MS/MS Analysis

For the sample preparation, the main components except borneolum syntheticum were dissolved in 50% methanol, followed by ultrasonic treatment, filtration, and concentration. The concentrated solution was then filtered through a micropore filter before injection and stored at 4°C until use.

For the chromatography analysis, we used a UPLC XBC18 column (2.1 mm × 100 mm, 1.8 μm) maintained at 30°C. UV detection was performed at a wavelength of 210 nm. The mobile phase consisted of methanol (D) and water (C) with

the following gradient program: 0–25 min 10% methanol (D); 25–35 min 40% methanol (D); 35–41 min 95% methanol (D); 41–45 min 10% methanol (D).

For the MS analysis, we utilized an electrospray ionization (ESI) source operating in both positive (ESI+) and negative (ESI-) ion modes. The parameters were as follows: temperature: 200°C; capillary voltage: 2.50 kV; nitrogen gas flow: 800 L/min; mass scanning range: m/z 50–1500.

GC-MS/MS Analysis

For the sample preparation, borneolum syntheticum was dissolved in methanol, and then was filtered through a micropore filter before injection and stored at 4°C until use.

For the chromatography analysis, we used an Agilent 19091S-433 column (30 m × 250 μm × 0.25 μm). Helium gas served as the carrier, flowing at a rate of 1.0 mL/min. The injection volume was 1 μL, with the inlet set at 260°C and a split ratio of 20:1. The temperature program was as follows: start at 60°C, hold for 1 minute; increase to 100°C at a rate of 8°C/min, maintain for 4 minutes; increase to 200°C at a rate of 30°C/min, maintain for 1 minute.

For the MS analysis, we used an electrospray ionization source operating in positive ion mode. The ion source temperature was set to 230°C. Both quadrupole 1 and quadrupole 2 temperatures were set at 150°C. The mass scanning range was from m/z 60 to 800 Da.

Statistical Method

Data analysis was accomplished using the SPSS 26.0 software. Shapiro–Wilk tests was performed to confirm that the data conformed to a Gaussian distribution. Then, all data were presented as mean ± standard deviation (SD). One-way analysis of variance (ANOVA) was employed for comparisons among multiple groups, followed by Dunnett's multiple comparison post hoc test for inter-group comparisons, with $p < 0.05$ being considered statistically significant.

Results

MHG Exerts Anti-Hemorrhoid Effect in COP-Induced HD Rat

To evaluate the anti-hemorrhoidal activity of MHG, we measured the ARC and assessed the macroscopic damage of the anorectal tissue. We found that COP-induced HD rats exhibited a significant increase in ARC (Figure 2A) and macroscopic severity score (Figure 2B) *(*$p < 0.001$), but both were significantly reduced following MHG treatment ($p < 0.01$, $p < 0.001$). TC exhibited effects similar to those of MHG. Morphological observations of the anorectal tissue further supported these results (Figure 2D). Bleeding is another important parameter for assessing hemorrhoidal symptoms, so we measured the Evans blue exudation rate in rats (Figure 2C). The results showed that in the COP group, the content of Evans blue in the anorectal tissue was significantly increased ($p < 0.001$), but it was markedly reduced following treatment with MHG and TC ($p < 0.001$). These results indicate that MHG has an obvious anti-hemorrhoid effect in COP-induced anorectal swelling, rectal mucosal injury, and rectal bleeding.

MHG Relieves Pathological Damage of Anorectal Tissue in COP-Induced HD Rat

The integrity of the intestinal epithelium is considered the first line of defense in the gastrointestinal tract and is essential for maintaining intestinal health. H&E staining results indicated that intestinal epithelium from the control group exhibited normal structure, with neatly arranged intestinal villi and intact mucosa. Conversely, COP caused severe tissue changes, including edema, disorganized villi, structural damage, and inflammatory cell infiltration. However, these pathological changes in the rectum were improved following MHG and TC treatments (Figure 3A).

Goblet cells are closely related to intestinal mucus secretion, playing an important role in maintaining intestinal function. PAS staining results revealed that in the control group, the number of goblet cells (stained purplish-red) was relatively high, widely distributed, and with intact structure. In the COP group, the number of goblet cells was reduced, and the structure was damaged. MHG treatment restored the normal structure and number of glomeruli to a certain extent (Figure 3B). These results suggest that MHG alleviates COP-induced edema of rectal tissue, villous structure damage, and goblet cell injury.

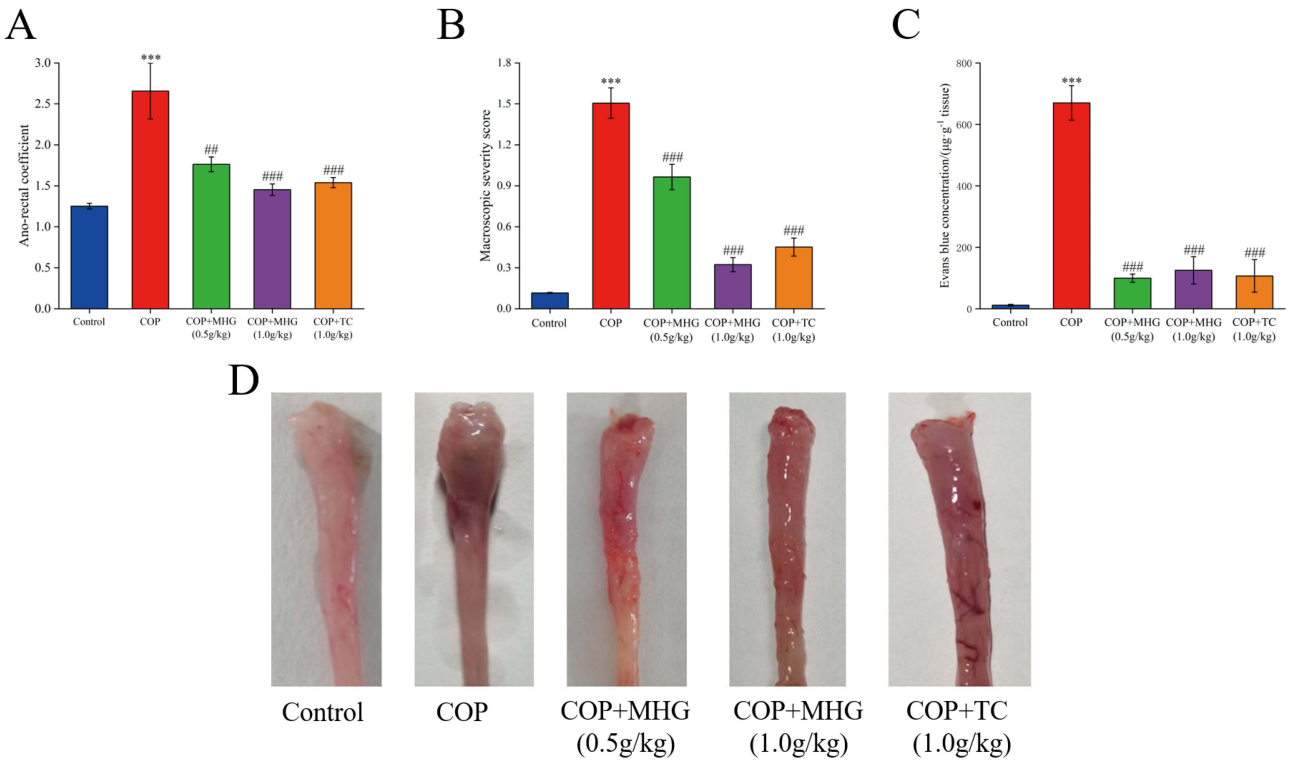

Figure 2 The anti-hemorrhoid effect of MHG. (**A**) Impact on anorectal coefficient. (**B**) Impact on macroscopic severity score. (**C**) Impact on Evans blue exudation. (**D**) Morphological observation of anorectal tissue. The mean ± SD is used to express the results.,$^{***}p < 0.001$, vs the control group; $^{###}p < 0.01$, $^{####}p < 0.001$, vs the COP group (n = 10 per group).

RNA-Seq Analysis Predicted Potential Mechanism of MHG in Treating HD

To explore the potential mechanisms of MHG in treating HD, we conducted RNA-seq analysis on rat anorectal tissues from three groups: Control, COP, and COP+MHG (1.0g/kg). The volcano plot analysis indicated that the COP group included a total of 3871 DEGs, with 2088 genes upregulated and 1783 genes downregulated compared to the Control group (Figure 4A). Interestingly, the COP+MHG (1.0g/kg) group displayed 1039 DEGs, including 538 upregulated and 501 downregulated genes relative to the COP group (Figure 4B). Venn diagram analysis further illustrated that among the 1783 downregulated genes induced by COP, 675 were reversed by MHG treatment (Figure 4C), and among the 2088 upregulated genes induced by COP, 1351 were reversed by MHG treatment (Figure 4D).

Functionally, we enriched 1525 GO terms of DEGs from the COP group vs COP+MHG (1.0g/kg) group. The GO enrichment analysis indicated that DEGs were primarily associated with processes such as positive regulation, inflammatory response, and signal transduction (Figure 4E). Furthermore, KEGG pathway enriched by DEGs in the COP vs COP+MHG (1.0g/kg) groups mainly include the PI3K-Akt, MAPK, and NF-κB signaling pathways, as well as pathways related to cell-cell interaction and calcium signaling (Figure 4F). These pathways are closely related to functions such as inflammation, cellular immunity, and apoptosis. These results suggest that MHG may affect pathways and reduce inflammatory response to exert anti-hemorrhoidal effects.

MHG Modulated the Inflammatory Response in COP-Induced HD Rats

Inflammatory response is a key feature in the pathology of HD. We measured the levels of TNF-α and IL-10 in the anorectal tissue of rats. The results showed that the level of pro-inflammatory cytokines TNF-α was markedly increased and the level of anti-inflammatory cytokines IL-10 was markedly decreased after COP-induced HD ($P < 0.05$, $P < 0.01$). However, MHG treatment significantly reduced the level of TNF-α and raised the level of IL-10 (Figure 5A–E), indicating that MHG may exert effects by modulating the inflammatory response in rats with hemorrhoids.

https://doi.org/10.2147/JIR.S526589

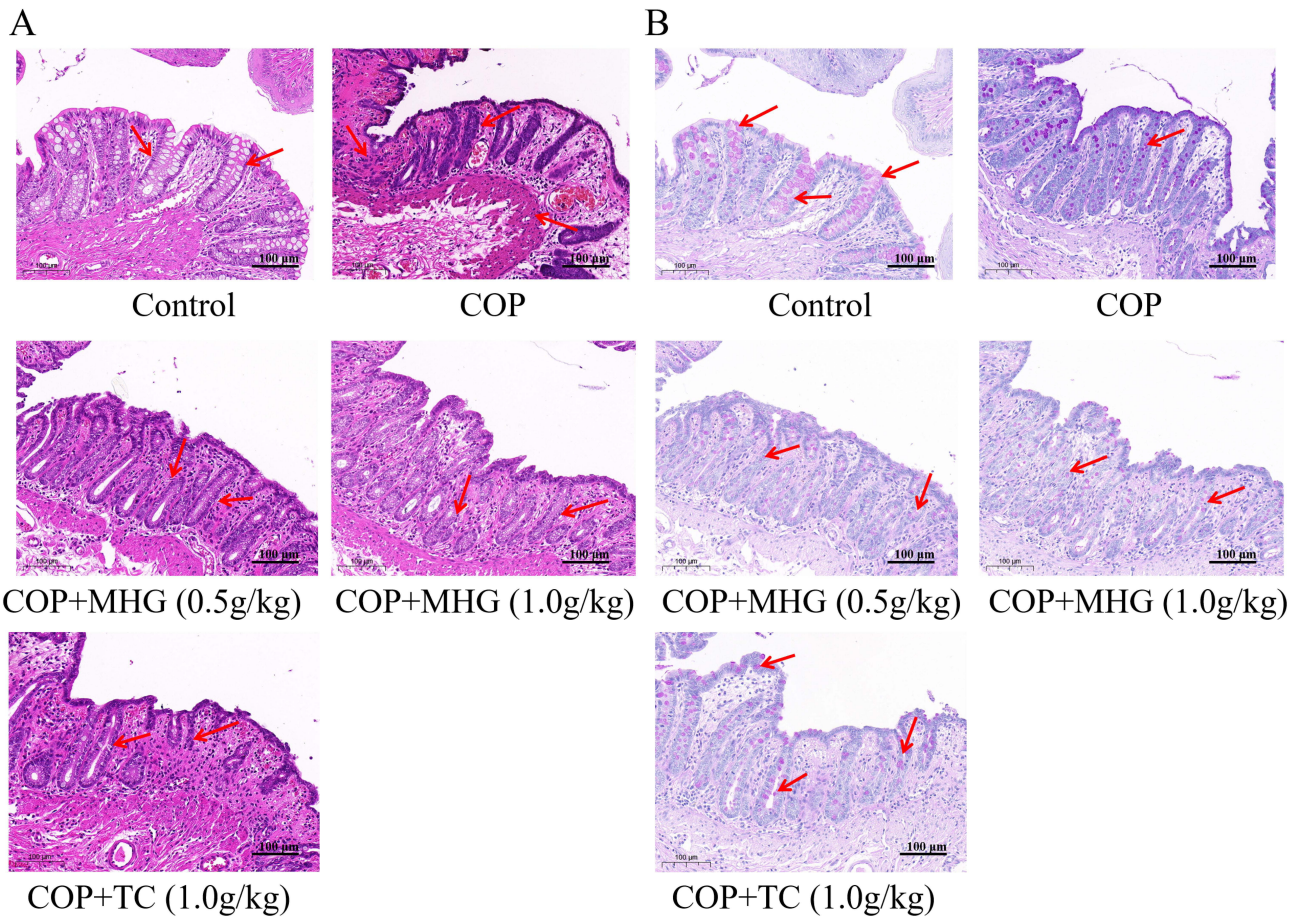

Figure 3 The effect of MHG on histopathology of anorectal tissue. (**A**) H&E (magnification ×100) and (**B**) PAS (magnification ×100) staining analysis.

MHG Inhibited COP-Induced Activation of the NLRP3 Inflammasome

Abnormal activation or dysregulation of NLRP3 inflammasome is the most common manifestation of inflammatory diseases. We hypothesized that the expression of inflammatory factors in hemorrhoids is related to the activation of NLRP3. As expected, the results showed (Figure 6A–D) that the AOD (average optical density) values of NLRP3, ASC, and Caspase-1 were markedly increased in HD rats. MHG significantly decreased the AOD values of NLRP3, ASC, and Caspase-1 ($P < 0.05$, $P < 0.01$). Moreover, Western blot analysis (Figure 6E–I) showed that in the COP group, there was a noticeable rise in the expression levels of NLRP3, ASC, Caspase-1, and IL-1β proteins ($P < 0.001$). The expression levels of NLRP3, ASC, Caspase-1, and IL-1β proteins significantly decreased after MHG treatment ($P < 0.01$, $P < 0.001$). These results suggest that MHG can inhibit NLRP3 inflammasome-related protein expression in COP-induced HD, thereby exerting anti-inflammatory effects.

MHG Regulated NF-κB Signaling Pathway to Attenuates Rectal Inflammation

The activation of the NLRP3 inflammasome is closely linked to the regulation of the NF-κB pathway. Building on the results of previous RNA-seq analysis, we further validated the impact of MHG on the expression of NF-κB pathway-related proteins. The results showed (Figure 7A–D) that the AOD values of p65 and p-p65 significantly increased, while the AOD value of IκBα markedly decreased in COP-induced HD rats ($P < 0.01$, $P < 0.001$). MHG treatment significantly reduced the AOD values of p65 and p-p65 and increased the AOD of IκBα ($P < 0.01$, $P < 0.001$). Additionally, the similar findings were also confirmed by Western blotting experiments (Figure 7E–G), suggesting that the NF-κB pathway may be the key signaling pathway for MHG to alleviate inflammation caused by HD.

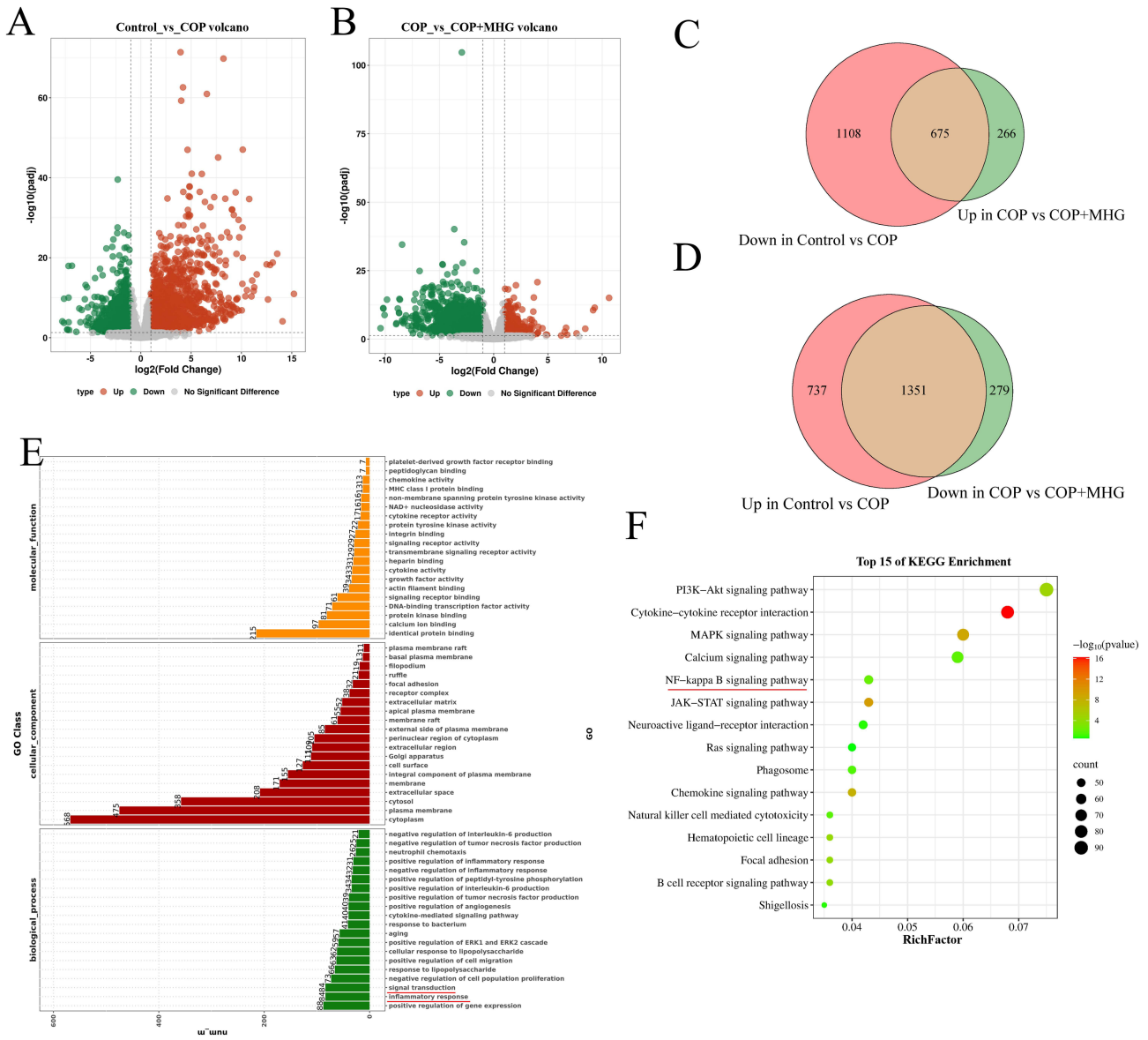

Figure 4 NF-κB mediated inflammatory response might be potential mechanism of MHG against HD (**A**) Volcano plot analysis of DEGs from the Control group and COP groups. (**B**) Volcano plot analysis of DEGs from the COP group and COP+MHG group. (**C**) Venn diagram illustrating DEGs downregulated in the Control vs COP comparison and upregulated in the COP vs COP+MHG comparison. (**D**) Venn diagram illustrating DEGs upregulated in the Control vs COP comparison and downregulated in the COP vs COP+MHG comparison. (**E**) The top 20 BP, CC and MF in GO enrichment analysis. (**F**) The top 15 key pathways in KEGG enrichment analysis (n = 3 per group).

MHG Phytochemical Analysis

To further characterize the primary chemical composition of MHG, we refer to the preparation process of MHG and the physical and chemical properties of each component. UPLC-QTOF-MS/MS was employed to analyze the stable mixtures, such as *Hamamelis mollis* Oliv, while GC-MS/MS was used for the analysis of volatile components, such as borneolum syntheticum, ensuring a comprehensive assessment of the formulation. Compound identification was performed through detailed comparison of fragmentation ions using the NIST library and a locally constructed natural products database. The total ion chromatograms were shown in the Figure 8. Finally, a total of 14 compounds were identified by UPLC-QTOF-MS/MS, including 3 tannin derivatives, 5 flavonoid derivatives, and 6 phenolic acid derivatives. A total of 6 compounds were identified by GC-MS/MS, including 4 terpenoids derivatives, 1 epoxy compound and 1 alkene compound. The information for the 20 compounds were presented in Table 1 and the structure of the 20 compounds were shown in Figure S3.

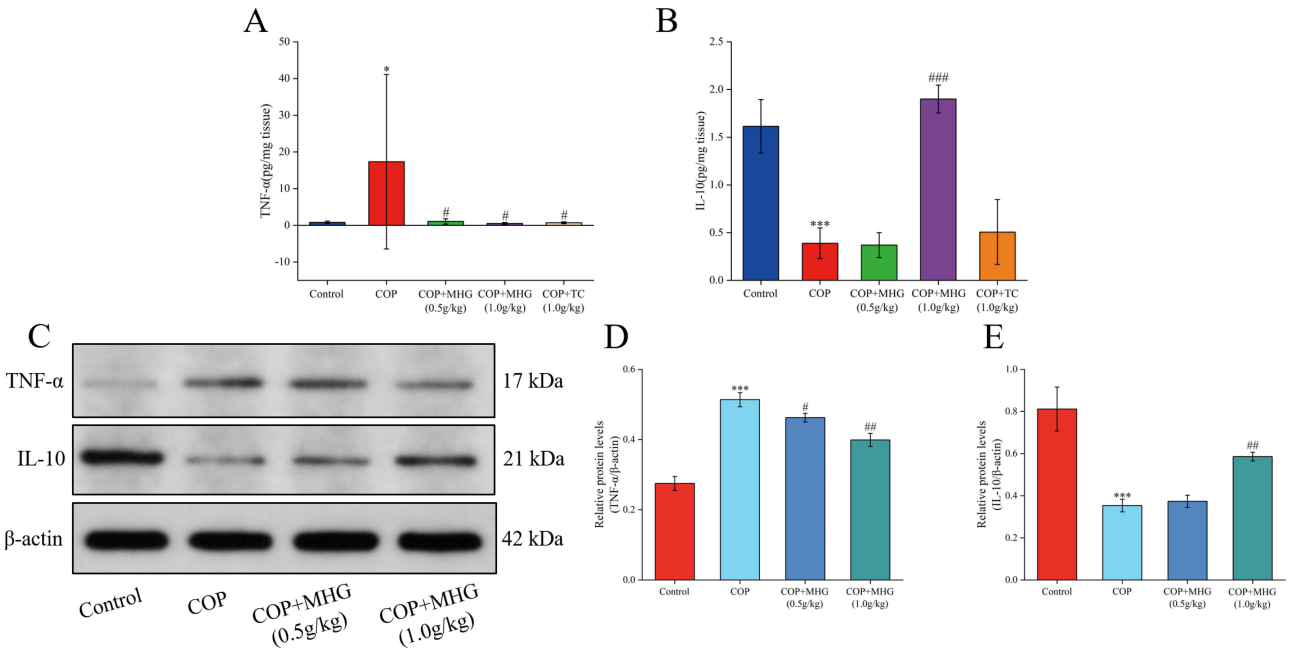

Figure 5 MHG can inhibit the production of TNF-α and promote the production of IL-10 in HD rats. Concentrations of TNF-α (**A**) and IL-10 (**B**) in anorectal tissues were analyzed by using ELISA (n=8 per group). (**C**) The representative Western blotting bands of TNF-α and IL-10. Protein relative expression level of TNF-α (**D**) and IL-10 (**E**) (n = 3 per group). The mean ± SD is used to express the results. *p<0.05,***p < 0.001, vs the control group; $^{\#}$p < 0.05, $^{\#\#}$p < 0.01, $^{\#\#\#}$p < 0.001 vs the COP group.

Discussion

Croton oil is primarily composed of fatty acids, triglycerides, and other components, with strong local irritant effect.[21] When croton oil comes into contact with the intestinal or anorectal skin, it induces a local inflammatory response, including congestion and edema, resulting in symptoms closely resembling clinical hemorrhoids, such as characteristic anal swelling and increased anal venous pressure.[22] In HD model, ARC usually serves as a key marker for assessing the extent of swelling in the rat anorectal region. Evans blue is a dye that, under normal conditions, circulates primarily within the bloodstream. However, when vascular permeability increases, it leaks into surrounding tissues, causing localized staining.[4] In this study, the topical application of COP to the rat anorectal mucosa successfully induced acute HD, as evidenced by significant increases in ARC, macroscopic severity scores, and Evans blue extravasation. Histopathological evaluation further revealed that COP-induced tissue abnormalities, including prominent edema, hemorrhage, inflammatory cell infiltration, and goblet cell damage, consistent with previous studies.[20] MHG treatment significantly improved these HD-related pathological parameters, including reductions in ARC, macroscopic severity scores, and Evans blue extravasation, as well as improvements in rectal tissue damage and cellular integrity. These results highlight the effective role of MHG in protecting the anorectal region from damage induced by COP. We further investigated the acute toxicity of MHG, and the results showed that administering MHG at a dose of 6.3 g/kg (approximately 10 times the clinical dose) in normal rats did not induce any abnormalities in the anorectal region or systemic toxicity (see Table S1), consistent with clinical observations, indicating its good safety and tolerability profile (see Figures S1 and S2).

Subsequently, transcriptomic analysis was employed to further explore the underlying mechanisms of MHG protection against HD. Transcriptome research provides a comprehensive approach to studying the relationship between transcriptional regulatory networks and phenotypes, revealing specific biological processes and molecular mechanisms involved in disease pathogenesis.[23] In this study, RNA-seq results confirmed that the therapeutic effect of MHG in HD was not regulated by individual genes, but rather by the co-expression of multiple genes. We further examined all DEGs, and found that some genes, such as IL-1β, TNF, p65, and NLRP3, have been associated with the pathogenesis of HD. For example, IL-1β and TNF, as key pro-inflammatory cytokines, play a pivotal role in driving inflammatory lesions, and their excessive release contributes to the development of HD.[24,25] p65, an important subunit of the NF-κB transcription

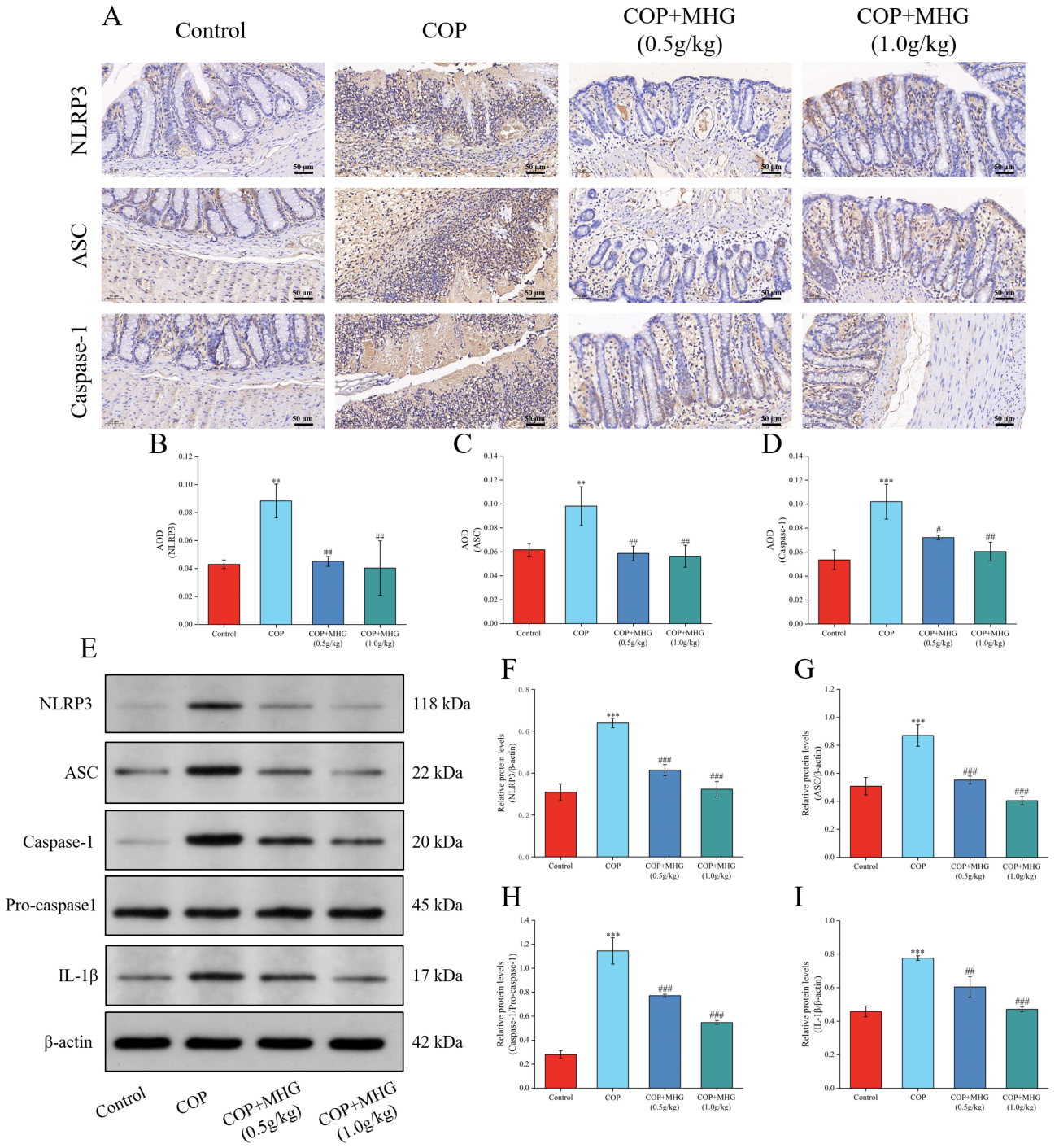

Figure 6 MHG can inhibit the activation of NLRP3 inflammasomes in anorectal tissue. (**A**) The representative anorectal tissue sections were stained with IHC (magnification × 160). AOD value of NLRP3 (**B**), ASC (**C**), Caspase-1 (**D**) in anorectal tissue sections. (**E**) The representative Western blotting bands of NLRP3, ASC, Caspase-1, Pro-caspase-1 and IL-1β. Protein relative expression level of NLRP3 (**F**), ASC (**G**), Caspase-1 (**H**) and IL-1β (**I**). The mean ± SD is used to express the result. **p<0.01,***p < 0.001, vs the control group; #p < 0.05, ##p < 0.01, ###p < 0.001, vs the COP group (n = 3 per group).

factor, mediates the transcription of inflammation-related genes, thereby enhancing the production of pro-inflammatory factors.[26] NLRP3, a crucial immune sensing molecule, when excessively activated, exacerbates local inflammation and increases the release of IL-1β.[27] Furthermore, through pathway enrichment analysis, we found that these genes were associated with inflammation pathways, such as the PI3K-Akt, MAPK, and NF-κB signaling pathways. Reportedly, the PI3K-Akt and MAPK signaling pathway is activated by various pro-inflammatory and plays a crucial role in cellular

https://doi.org/10.2147/JIR.S526589

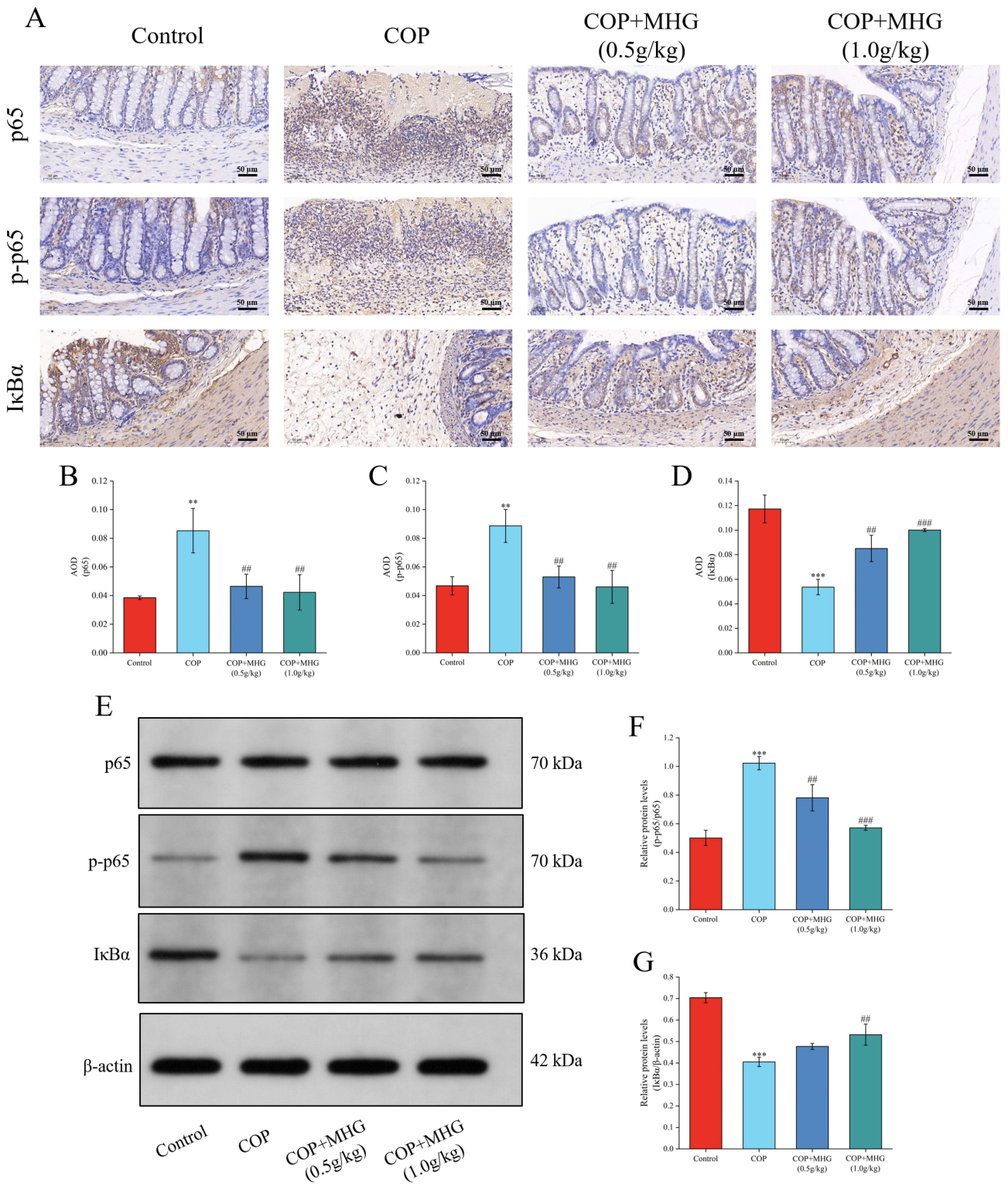

Figure 7 MHG can modulate the NF-κB signaling pathway in anorectal tissue. (**A**) The representative anorectal tissue sections were stained with IHC (magnification ×160). AOD value of p65 (**B**), p-p65 (**C**) and IκBα (**D**) in anorectal tissue sections. (**E**) The representative Western blotting bands of p65, p-p65 and IκBα. Protein relative expression level of p-p65 (**F**) and of IκBα (**G**). The mean ± SD is used to express the results., **p<0.01,***p < 0.001, vs the control group; ##p < 0.01, ###p < 0.001, vs the COP group (n = 3 per group).

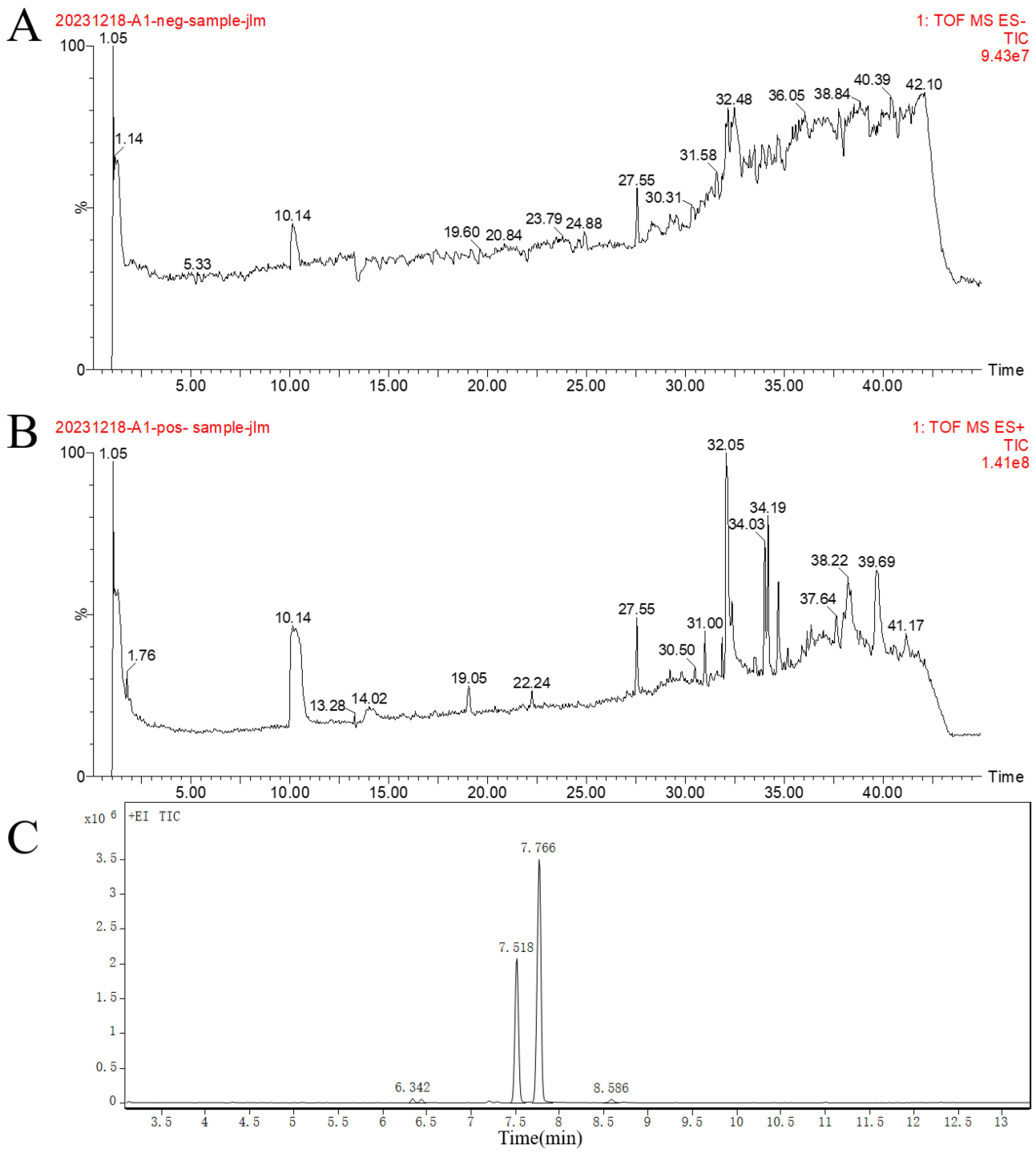

Figure 8 Phytochemical composition analysis of MHG. Total ion flow chromatograms of MHG sample analyzed by UPLC-QTOF-MS/MS in negative (**A**) and positive (**B**) ion modes. (**C**) Total ion chromatogram of MHG sample analyzed by GC-MS/MS.

processes involved in inflammation[28,29]. Furthermore, Piazza et al demonstrated that *Hamamelis mollis* Oliv extract can suppress the release of inflammatory mediators in skin by inhibiting NF-κB transcription, providing the first evidence of *Hamamelis mollis* Oliv inhibiting the NF-κB signaling pathway to mitigate inflammation.[30] These results showed that MHG may inhibit inflammation response by regulating the NF-κB signaling pathway, but it requires further experimental validation.

https://doi.org/10.2147/JIR.S526589

Table 1 The Structure and Information of 20 Chemical Compounds Identified in MHG

Classification	Compound	t_R (min)	Molecular Formula	Pseudo Molecular Ion	Polarity
Identified by UPLC-QTOF-MS/MS					
Tannins derivatives	Trigalloyl hexose	29.22	$C_{27}H_{24}O_{18}$	635.46	$M-H^-$
	Tetragalloyl hexose	38.22	$C_{34}H_{28}O_{22}$	789.58	$M+H^+$
	Hamamelitannin	20.47	$C_{22}H_{22}O_{12}$	479.41	$M+H^+$
Flavonoids derivatives	Rutin	29.22	$C_{27}H_{30}O_{16}$	611.53	$M+H^+$
	Gallocatechin	31.08	$C_{15}H_{14}O_7$	305.26	$M-H^-$
	Kaempferol 3-O-glucoside	33.26	$C_{21}H_{20}O_{11}$	447.37	$M-H^-$
	Naringenin	37.76	$C_{15}H_{12}O_5$	271.24	$M-H^-$
	Kaempferol	39.25	$C_{15}H_{10}O_6$	285.23	$M-H^-$
Phenolic acids derivatives	Protocatechuic acid	1.76	$C_7H_6O_4$	155.11	$M+H^+$
	Ethyl gallate	12.07	$C_9H_{10}O_5$	199.18	$M+H^+$
	Ferulic acid	13.15	$C_{10}H_{10}O_4$	195.19	$M+H^+$
	Theogallin	1.05	$C_{14}H_{16}O_{10}$	343.27	$M-H^-$
	Chlorogenic acid	37.64	$C_{16}H_{18}O_9$	355.32	$M+H^+$
	Gallic acid	41.32	$C_7H_6O_5$	169.11	$M-H^-$
Identified by GC-MS/MS					
Epoxy compound	4-Ethyl-3-oxabicyclo4.4.0decane	6.342	$C_{11}H_{20}O$	169.15	$M+H^+$
Terpenoids derivatives	(+)-Fenchol	6.441	$C_{10}H_{18}O$	155.14	$M+H^+$
	Camphor	7.203	$C_{10}H_{16}O$	153.12	$M+H^+$
	(+)-Borneol	7.518	$C_{10}H_{18}O$	155.14	$M+H^+$
	(-)-Borneol	7.775	$C_{10}H_{18}O$	155.14	$M+H^+$
Alkene compound	2,5-Dimethyl-2,4-hexadiene	8.586	C_8H_{14}	111.11	$M+H^+$

Numerous studies have shown that croton oil induces the migration of inflammatory cells, promotes the release of pro-inflammatory substances (eg TNF-α), and inhibits the production of anti-inflammatory substances (eg IL-10), ultimately triggering an inflammatory response.[31,32] In the present study, we demonstrated that MHG treatment suppressed the inflammatory response in COP-induced HD by downregulating TNF-α and upregulating IL-10 levels. Furthermore, increasing evidence underscores the association between TNF-α, IL-10, and NLRP3 inflammasome activation. Excessive TNF-α can trigger the activation and assembly of the NLRP3 inflammasome in the rectum, leading to the release of additional pro-inflammatory cytokines, such as IL-1β, which in turn drives a sustained inflammatory response, exacerbating the progression of HD.[33–35] In contrast to TNF-α, IL-10 can activate downstream signaling pathways via its receptor, reducing the levels of pro-inflammatory cytokines (eg TNF-α and IL-1β), thus inhibiting the excessive activation of the NLRP3 inflammasome, mitigating the inflammatory response, and promoting tissue repair.[36,37] These findings suggest an important role of the NLRP3 inflammasome in rectal inflammation, and our subsequent research focused on elucidating the effect of MHG in regulating NLRP3 inflammasome activation. The NLRP3 inflammasome is a multimeric complex consisting of NLRP3, ASC, and caspase-1.[38] It has been reported that NLRP3 inflammasome activation plays an important role in intestinal inflammatory diseases such as ulcerative colitis, Crohn's disease, and irritable bowel syndrome.[39,40] Furthermore, excessive activation of the NLRP3 leads to the cleavage of pro-caspase-1 into active caspase-1, which further catalyzes the production and release of IL-1β and IL-18, ultimately leading to the development of rectal inflammation.[41] Importantly, our results showed that MHG significantly reduced the protein expression of NLRP3 and downstream cascades in the anorectal tissue of COP-induced HD rats.

In addition, growing study has demonstrated that the activation of NF-κB pathway can enhance the expression of NLRP3, promoting the formation of the NLRP3 inflammasome.[42,43] Consequently, inhibiting the NF-κB pathway to reduce NLRP3 inflammasome activation may be a promising therapeutic approach for inflammatory bowel diseases, including HD. For example, Wang et al reported that inhibition of the NF-κB/NLRP3 axis alleviates DDS-induced experimental colitis.[44] Zhang et al demonstrated that inhibiting the NF-κB/NLRP3 pathway mitigates diarrhea-

predominant irritable bowel syndrome.[45] Moreover, IκBα, as a negative feedback regulator of NF-κB activity, mediates the activation of the IκB kinase complex and the phosphorylation of p65, preventing excessive activation of NF-κB.[46,47] Increasing the expression of IκBα has been proposed as a potential strategy to inhibit the activation of the NF-κB pathway.[48] Similarly, our results suggested that MHG treatment significantly increased the expression of IκBα protein while decreasing the phosphorylation of p65 protein in COP-induced HD rats, indicating that MHG may alleviate rectal inflammation and reduce intestinal mucosal damage by inhibiting the activation of the NF-κB signaling pathway.

To identify the active components of MHG, a comprehensive phytochemical characterization was conducted using UPLC-QTOF-MS/MS and GC-MS/MS. A total of 20 potential bioactive compounds were identified. Among them, some compounds exhibit potent anti-inflammatory properties, potentially contributing to MHG protection against HD. For example, Hamamelitannin demonstrated dual antioxidant and anti-inflammatory capacities through radical scavenging and protein precipitation mechanisms.[49,50] Kaempferol, a natural flavonol in various plant species, has been shown to inhibit the activation of the NF-κB pathway and the overexpression of inflammatory mediators, thereby suppressing inflammatory responses and improving intestinal barrier integrity.[51] Rutin and Naringenin are capable of downregulating the NLRP3/NF-κB pathway, inhibiting LPS-induced inflammatory responses.[52,53] Additionally, more studies showed that phenolic acid compounds can alleviate stress-induced intestinal oxidative stress and inflammatory responses, thereby promoting gut health.[54–56] In summary, the therapeutic effects of MHG in treating HD likely result from the interactions and coordination of multiple constituents, most of which exhibit potent anti-inflammatory effects, aligning with our research findings.

While these promising findings, there are several limitations worth noting. Firstly, this study demonstrated the protective effects of MHG and its ability to inhibit retcal inflammation using a normal rat model, employing more advanced techniques, such as gene editing, could deepen our understanding of the molecular mechanisms through which MHG alleviates hemorrhoids and suppresses inflammatory responses. Furthermore, although this study identified several potential bioactive components of MHG, further investigation is needed to determine the direct molecular targets of these compounds. Such research will be crucial for the development of formulations based on these active ingredients and could expand the clinical treatment options for HD. These will be key areas of focus in our future research.

Conclusions

In summary, we provide initial evidence of the protective effect of MHG against COP-induced HD in rats, possibly achieved by suppressing the activation of NLRP3 inflammasome via the NF-κB signaling pathway, ultimately alleviating COP-induced hemorrhoids. The therapeutic benefits of MHG were linked with the reduction of tissue edema, restoration of the intestinal mucosal barrier, and mitigation of rectal inflammation. While these findings are significant, employing more advanced methodologies may provide a more comprehensive understanding of MHG's protective effects on the rectum and its capacity to suppress inflammation. Furthermore, given the current limitations of available clinical therapies for HD, investigating the safety and efficacy of MHG in combination with other medications is crucial for expanding its therapeutic potential. Lastly, this study focused on the therapeutic effects of MHG in acute hemorrhoids, and the short observation period may be a limitation. In future work, we plan to extend the treatment duration to 5–7 days to further evaluate its long-term efficacy and potential adverse effects in HD.

Data Sharing Statement

The data that support the findings of this study are available from the corresponding author upon reasonable request.

Ethical Approval

All experiments were conducted in accordance with the ARRIVE (Animal in Research: In Vivo Experiments) guidelines. The animals were treated in accordance with the Guidelines for Ethical Review of Experimental Animal Welfare (GB/T35892-2018) issued by China. The animal experiment was approved by Animal Ethics Committee of Hubei University of Chinese Medicine (Permission No. SYXK2017-0067-ZYZYZX2023-031 and SYXK2017-0067-ZYZYZX2023-051).

Author Contributions

All authors made a significant contribution to the work reported, whether that is in the conception, study design, execution, acquisition of data, analysis and interpretation, or in all these areas; took part in drafting, revising or critically reviewing the article; gave final approval of the version to be published; have agreed on the journal to which the article has been submitted; and agree to take responsibility and be accountable for the contents of the article.

Funding

The author(s) declares financial support for research, authorship, and/or publication of this article. This study was supported by the Peking University and Ma Yinglong Pharmaceutical Group Postdoctoral Joint Workstation (H2023070).

Disclosure

The authors declare no conflict of interest, financial or otherwise.

References

1. Zheng T, Ellinghaus D, Juzenas S, et al. Genome-wide analysis of 944,133 individuals provides insights into the etiology of haemorrhoidal disease. *Gut*. 2021;70(8):1538–1549. doi:10.1136/gutjnl-2020-323868
2. Yang JY, Peery AF, Lund JL, Pate V, Sandler RS. Burden and cost of outpatient hemorrhoids in the United States employer-insured population, 2014. *Am J Gastroenterol*. 2019;114(5):798–803. doi:10.14309/ajg.0000000000000143
3. Davis BR, Lee-Kong SA, Migaly J, Feingold DL, Steele SR. The American society of colon and rectal surgeons clinical practice guidelines for the management of hemorrhoids. *Dis Colon Rectum*. 2018;61(3):284–292. doi:10.1097/DCR.0000000000001030
4. Zhang H, Yao XY, Zhang DF, et al. Anti-hemorrhoidal activity of Lian-Zhi-San, a traditional Chinese medicine, in an experimental hemorrhoidal model in rats. *J Integr Med*. 2021;19(1):42–49. doi:10.1016/j.joim.2020.09.006
5. Nasr M, Cavalu S, Saber S, et al. Canagliflozin-loaded chitosan-hyaluronic acid microspheres modulate AMPK/NF-κB/NLRP3 axis: a new paradigm in the rectal therapy of ulcerative colitis. *Biomed Pharmacother*. 2022;153:113409. doi:10.1016/j.biopha.2022.113409
6. Dekker L, Han-Geurts IJM, Rørvik HD, van Dieren S, Bemelman WA. Rubber band ligation versus haemorrhoidectomy for the treatment of grade II-III haemorrhoids: a systematic review and meta-analysis of randomised controlled trials. *Tech Coloproctol*. 2021;25(6):663–674. doi:10.1007/s10151-021-02430-x
7. Albuquerque A. Rubber band ligation of hemorrhoids: a guide for complications. *World J Gastrointest Surg*. 2016;8(9):614–620. doi:10.4240/wjgs.v8.i9.614
8. Sheikh P, Lohsiriwat V, Shelygin Y. Micronized purified flavonoid fraction in hemorrhoid disease: a systematic review and meta-analysis. *Adv Ther*. 2020;37(6):2792–2812. doi:10.1007/s12325-020-01353-7
9. Liang Y, Ren T, Li R, et al. Natural products with potential effects on hemorrhoids: a review. *Molecules*. 2024;29(11):2673. doi:10.3390/molecules29112673
10. Razdar S, Panahi Y, Mohammadi R, Khedmat L, Khedmat H. Evaluation of the efficacy and safety of an innovative flavonoid lotion in patients with haemorrhoid: a randomised clinical trial. *BMJ Open Gastroenterol*. 2023;10(1):e001158. doi:10.1136/bmjgast-2023-001158
11. Amaturo A, Meucci M, Mari FS. Treatment of haemorrhoidal disease with micronized purified flavonoid fraction and sucralfate ointment. *Acta Biomed*. 2020;91(1):139–141. doi:10.23750/abm.v91i1.9361
12. Zhu BH, Li LP, Xu DG. Clinical observation of Chinese herbal fumigation and washing combined with mayinglong musk hemorrhoids ointment in treating mixed hemorrhoids of dampheat inflowing downward type. *Chin Naturopathy*. 2023;31(19):37–40. doi:10.19621/j.cnki.11-3555/r.2023.1913
13. Natella F, Guantario B, Ambra R, et al. Human metabolites of hamaforton™ (*Hamamelis virginiana* L. Extract) modulates fibroblast extracellular matrix components in response to UV-A irradiation. *Front Pharmacol*. 2021;12:747638. doi:10.3389/fphar.2021.747638
14. Wang J, Yan M, Zhang M, Jiang M, Bai G. Study on the mechanism of "guiding action" of borneol in Suxiaojiuxin pills. *Acta Pharm Sin*. 2022;57(3):700–706. Chinese. doi:10.16438/j.0513-4870.2021-1122
15. Bansod S, Chilvery S, Saifi MA, Das TJ, Tag H, Godugu C. Borneol protects against cerulein-induced oxidative stress and inflammation in acute pancreatitis mice model. *Environ Toxicol: Int J*. 2021;36(4):530–539. doi:10.1002/tox.23058
16. Hu C, Liu W, Long L, et al. Microenvironment-responsive multifunctional hydrogels with spatiotemporal sequential release of tailored recombinant human collagen type III for the rapid repair of infected chronic diabetic wounds. *J Mater Chem B*. 2021;29(47):9684–9699. doi:10.1039/d1tb02170b
17. Long LY, Liu W, Li L, et al. Dissolving microneedle-encapsulated drug-loaded nanoparticles and recombinant humanized collagen type III for the treatment of chronic wound via anti-inflammation and enhanced cell proliferation and angiogenesis. *Nanoscale*. 2022;14(4):1285–1295. doi:10.1039/d1nr07708b
18. Ai Z, Yuan D, Cai J, Dong R, Liu W, Zhou D. Mechanism of medical hemorrhoid gel in relieving pruritus ani via inhibiting the activation of JAK2/STAT3 pathway. *Front Med*. 2024;11:1487531. doi:10.3389/fmed.2024.1487531
19. Dey YN, Wanjari MM, Kumar D, Lomash V, Jadhav AD. Curative effect of Amorphophallus paeoniifolius tuber on experimental hemorrhoids in rats. *J Ethnopharmacol*. 2016;192:183–191. doi:10.1016/j.jep.2016.07.042
20. Apaydin Yildirim B, Aydin T, Kordali S, Yildirim S, Cakir A, Yildirim F. Antihemorrhoidal activity of organic acids of *Capsella bursa-pastoris* on croton oil-induced hemorrhoid in rats. *J Food Biochem*. 2020;44(9):e13343. doi:10.1111/jfbc.13343
21. Pegoraro NS, Camponogara C, Cruz L, Oliveira SM. Oleic acid exhibits an expressive anti-inflammatory effect in croton oil-induced irritant contact dermatitis without the occurrence of toxicological effects in mice. *J Ethnopharmacol*. 2021;267:113486. doi:10.1016/j.jep.2020.113486

22. Dönmez C, Yalçın FN, Boyacıoğlu Ö, et al. From nutrition to medicine: assessing hemorrhoid healing activity of *Solanum melongena* L. via *in vivo* experimental models and its major chemicals. *J Ethnopharmacol*. 2020;261:113143. doi:10.1016/j.jep.2020.113143
23. Ni T, Sun Y, Li Z, et al. Integrated transcriptome analysis reveals novel molecular signatures for schizophrenia characterization. *Adv Sci*. 2025;12 (2):e2407628. doi:10.1002/advs.202407628
24. Gerassy-Vainberg S, Blatt A, Danin-Poleg Y, et al. Radiation induces proinflammatory dysbiosis: transmission of inflammatory susceptibility by host cytokine induction. *Gut*. 2018;67(1):97–107. doi:10.1136/gutjnl-2017-313789
25. Jo M, Lee J, Kim HG, et al. Anti-inflammatory effect of Barringtonia angusta methanol extract is mediated by targeting of Src in the NF-κB signalling pathway. *Pharm Biol*. 2021;59(1):799–810. doi:10.1080/13880209.2021.1938613
26. Sun SC. The non-canonical NF-κB pathway in immunity and inflammation. *Nat Rev Immunol*. 2017;17(9):545–558. doi:10.1038/nri.2017.52
27. Hafez HM, Ibrahim MA, Yehia Abdelzaher W, Gad AA, Mohammed Naguib Abdel Hafez S, Abdel-Gaber SA. Protective effect of mirtazapine against acetic acid-induced ulcerative colitis in rats: role of NLRP3 inflammasome pathway. *Int Immunopharmacol*. 2021;101(Pt A):108174. doi:10.1016/j.intimp.2021.108174
28. Jin J, Zhong Y, Long J, et al. Ginsenoside Rg1 relieves experimental colitis by regulating balanced differentiation of Tfh/Treg cells. *Int Immunopharmacol*. 2021;100:108133. doi:10.1016/j.intimp.2021.108133
29. Yang S, Li W, Bai X, et al. Ginseng-derived nanoparticles alleviate inflammatory bowel disease via the TLR4/MAPK and p62/Nrf2/Keap1 pathways. *J Nanobiotechnology*. 2022;22(1):48. doi:10.1186/s12951-024-02313-x
30. Piazza S, Martinelli G, Magnavacca A, et al. Unveiling the ability of witch hazel (*Hamamelis virginiana* L.) bark extract to impair keratinocyte inflammatory cascade typical of atopic eczema. *Int J Mol Sci*. 2022;23(16):9279. doi:10.3390/ijms23169279
31. Pekacar S, Özüpek B, Akkol EK, Taştan H, Ersan H, Orhan DD. Identification of bioactive components on antihemorrhoidal activity of *Cistus laurifolius* L. using RP-HPLC and LC-QTOF-MS. *J Ethnopharmacol*. 2024;319(Pt 1):117122. doi:10.1016/j.jep.2023.117122
32. de Araújo ERD, Félix-Silva J, Xavier-Santos JB, et al. Local anti-inflammatory activity: topical formulation containing Kalanchoe brasiliensis and Kalanchoe pinnata leaf aqueous extract. *Biomed Pharmacother*. 2019;113:108721. doi:10.1016/j.biopha.2019.108721
33. Cosin-Roger J, Simmen S, Melhem H, et al. Hypoxia ameliorates intestinal inflammation through NLRP3/mTOR downregulation and autophagy activation. *Nat Commun*. 2017;8(1):98. doi:10.1038/s41467-017-00213-3
34. Cai B, Zhao J, Zhang Y, et al. USP5 attenuates NLRP3 inflammasome activation by promoting autophagic degradation of NLRP3. *Autophagy*. 2022;18(5):990–1004. doi:10.1080/15548627.2021.1965426
35. Fei X, Chen S, Li L, et al. Helicobacter pylori infection promotes M1 macrophage polarization and gastric inflammation by activation of NLRP3 inflammasome via TNF/TNFR1 axis. *Cell Commun Signal*. 2025;23(1):6. doi:10.1186/s12964-024-02017-7
36. Wke I, Hoshi N, Shouval DS, Snapper S, Medzhitov R. Anti-inflammatory effect of IL-10 mediated by metabolic reprogramming of macrophages. *Science*. 2017;356(6337):513–519. doi:10.1126/science.aal3535
37. Kim TH, Yang K, Kim M, Kim HS, Kang JL. Apoptosis inhibitor of macrophage (AIM) contributes to IL-10-induced anti-inflammatory response through inhibition of inflammasome activation. *Cell Death Dis*. 2021;12(1):19. doi:10.1038/s41419-020-03332-w
38. Bauer C, Duewell P, Mayer C, et al. Colitis induced in mice with dextran sulfate sodium (DSS) is mediated by the NLRP3 inflammasome. *Gut*. 2010;59(9):1192–1199. doi:10.1136/gut.2009.197822
39. Mehto S, Jena KK, Nath P, et al. The Crohn's disease risk factor IRGM limits NLRP3 inflammasome activation by impeding its assembly and by mediating its selective autophagy. *Mol Cell*. 2019;73(3):429–445.e7. doi:10.1016/j.molcel.2018.11.018
40. Coll RC, Schroder K, Pelegrín P. NLRP3 and pyroptosis blockers for treating inflammatory diseases. *Trends Pharmacol Sci*. 2022;43(8):653–668. doi:10.1016/j.tips.2022.04.003
41. Liu H, Chen R, Wen S, et al. Tea (Camellia sinensis) ameliorates DSS-induced colitis and liver injury by inhibiting TLR4/NF-κB/NLRP3 inflammasome in mice. *Biomed Pharmacother*. 2023;158:114136. doi:10.1016/j.biopha.2022.114136
42. Yu H, Lin L, Zhang Z, Zhang H, Hu H. Targeting NF-κB pathway for the therapy of diseases: mechanism and clinical study. *Signal Transduct Target Ther*. 2020;5(1):209. doi:10.1038/s41392-020-00312-6
43. Li S, Fang Y, Zhang Y, et al. Microglial NLRP3 inflammasome activates neurotoxic astrocytes in depression-like mice. *Cell Rep*. 2022;41 (4):111532. doi:10.1016/j.celrep.2022.111532
44. Wang S, Lin Y, Yuan X, Li F, Guo L, Wu B. REV-ERBα integrates colon clock with experimental colitis through regulation of NF-κB/NLRP3 axis. *Nat Commun*. 2018;9(1):4246. doi:10.1038/s41467-018-06568-5
45. Zhang S, Tian D, Xia Z, et al. Chang-Kang-Fang alleviates diarrhea predominant irritable bowel syndrome (IBS-D) through inhibiting TLR4/NF-κB/NLRP3 pathway. *J Ethnopharmacol*. 2024;330:118236. doi:10.1016/j.jep.2024.118236
46. Lee HJ, Seo HS, Kim GJ, et al. Houttuynia cordata Thunb inhibits the production of pro-inflammatory cytokines through inhibition of the NFκB signaling pathway in HMC-1 human mast cells. *Mol Med Rep*. 2013;8(3):731–736. doi:10.3892/mmr.2013.1585
47. Moon PD, Lee BH, Jeong HJ, et al. Use of scopoletin to inhibit the production of inflammatory cytokines through inhibition of the IkappaB/NF-kappaB signal cascade in the human mast cell line HMC-1. *Eur J Pharmacol*. 2007;555(2–3):218–225. doi:10.1016/j.ejphar.2006.10.021
48. Son M, Wang AG, Tu HL, et al. NF-κB responds to absolute differences in cytokine concentrations. *Sci Signal*. 2021;14(666):eaaz4382. doi:10.1126/scisignal.aaz4382
49. Masaki H, Atsumi T, Sakurai H. Protective activity of hamamelitannin on cell damage induced by superoxide anion radicals in murine dermal fibroblasts. *Biol Pharm Bull*. 1995;18(1):59–63. doi:10.1248/bpb.18.59
50. Habtemariam S. Hamamelitannin from Hamamelis virginiana inhibits the tumour necrosis factor-alpha (TNF)-induced endothelial cell death in vitro. *Toxicon*. 2002;40(1):83–88. doi:10.1016/S0041-0101(01)00195-7
51. Bian Y, Lei J, Zhong J, et al. Kaempferol reduces obesity, prevents intestinal inflammation, and modulates gut microbiota in high-fat diet mice. *J Nutr Biochem*. 2022;99:108840. doi:10.1016/j.jnutbio.2021.108840
52. Muvhulawa N, Dludla PV, Ziqubu K, et al. Rutin ameliorates inflammation and improves metabolic function: a comprehensive analysis of scientific literature. *Pharmacol Res*. 2022;178:106163. doi:10.1016/j.phrs.2022.106163
53. Wang Q, Ou Y, Hu G, et al. Naringenin attenuates non-alcoholic fatty liver disease by down-regulating the NLRP3/NF-κB pathway in mice. *Br J Pharmacol*. 2020;177(8):1806–1821. doi:10.1111/bph.14938
54. Liu Y, Qi Y, Chen X, et al. Phenolic compounds and antioxidant activity in red- and in green-fleshed kiwifruits. *Food Res Int*. 2019;116:291–301. doi:10.1016/j.foodres.2018.08.038

55. Li D, Rui YX, Guo SD, Luan F, Liu R, Zeng N. Ferulic acid: a review of its pharmacology, pharmacokinetics and derivatives. *Life Sci*. 2021;284:119921. doi:10.1016/j.lfs.2021.119921
56. Yang K, Deng X, Jian S, et al. Gallic acid alleviates gut dysfunction and boosts immune and antioxidant activities in puppies under environmental stress based on microbiome-metabolomics analysis. *Front Immunol*. 2022;12:813890. doi:10.3389/fimmu.2021.813890